

The Crystal Structure of Phosphinothricin in the Active Site of Glutamine Synthetase Illuminates the Mechanism of Enzymatic Inhibition[†]

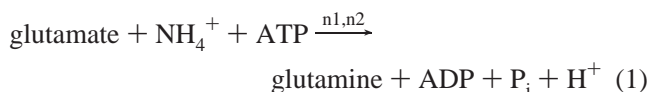
Harindarpal S. Gill and David Eisenberg*

UCLA-DOE Lab of Structural Biology and Molecular Medicine, Departments of Chemistry and Biochemistry and Biological Chemistry, Box 951570, University of California, Los Angeles, California 90095-1570

Received October 20, 2000; Revised Manuscript Received December 11, 2000

ABSTRACT: Phosphinothricin is a potent inhibitor of the enzyme glutamine synthetase (GS). The resolution of the native structure of GS from *Salmonella typhimurium* has been extended to 2.5 Å resolution, and the improved model is used to determine the structure of phosphinothricin complexed to GS by difference Fourier methods. The structure suggests a noncovalent, dead-end mechanism of inhibition. Phosphinothricin occupies the glutamate substrate pocket and stabilizes the Glu327 flap in a position which blocks the glutamate entrance to the active site, trapping the inhibitor on the enzyme. One oxygen of the phosphinyl group of phosphinothricin appears to be protonated, because of its proximity to the carboxylate group of Glu327. The other phosphinyl oxygen protrudes into the negatively charged binding pocket for the substrate ammonium, disrupting that pocket. The distribution of charges in the glutamate binding pocket is complementary to those of phosphinothricin. The presence of a second ammonium binding site within the active site is confirmed by its analogue thallos ion, marking the ammonium site and its protein ligands. The inhibition of GS by methionine sulfoximine can be explained by the same mechanism. These models of inhibited GS further illuminate its catalytic mechanism.

Glutamine synthetase (GS)¹ catalyzes the ATP-dependent condensation of ammonium and glutamate to form glutamine, ADP, and free phosphate. This biosynthetic reaction may be written



where n1 and n2 are either magnesium or manganese ions. The reaction proceeds through the tightly bound, activated intermediate γ -glutamyl phosphate (Glu~P) (1–5) formed when the terminal phosphate of ATP is transferred to the carboxylate side chain of the substrate glutamate (4). In a second step, a bound ammonium ion is deprotonated, forming ammonia which attacks the carbonyl carbon of Glu~P to form a tetrahedral intermediate at the transition state and subsequently releases free phosphate to yield glutamine (4).

The structure of glutamine synthetase (GS) from a mutant *Salmonella typhimurium* strain, unable to adenylate GS (6), was initially determined to 3.5 Å resolution by X-ray crystallography (7). The structure was refined subsequently

and the resolution extended to 2.9 Å (8, 9). *Salmonella typhimurium* GS has a molecular mass of 620 kDa and is a dodecamer with 622 symmetry (7, 10), formed from two hexameric rings stacked on top of one another. Each of the 12 active sites is formed between every two adjacent subunits within a ring and is described as a “bifunnel”. ATP enters the bifunnel from the exposed top surface of the dodecamer, near the 6-fold axis of symmetry. Glutamate enters the bifunnel at the bottom, the interface of the hexameric rings, near the 2-fold axes. At the joint of the bifunnel are the n1 and n2 divalent cation binding sites.

Structural changes in GS along the reaction pathway of reaction 1 have been inferred in part from its inhibition by phosphinothricin (PPT) and methionine sulfoximine (MetSox). As illustrated in Figure 1, PPT and MetSox are structural analogues of glutamate and compete with glutamate for binding in the active site (5, 11). In the presence of ATP, either is phosphorylated by GS and becomes an essentially irreversible, noncovalent inhibitor of the enzyme (12, 13). The tight binding has been attributed to the apparent resemblance of the phosphorylated inhibitors with the tetrahedral adduct at the transition state in reaction 1 (14–16). In the case of MetSox, where the *S*-isomer is the more inhibitory isomer (17), the nitrogen (Nε) of the sulfonimide group forms a covalent linkage to ³²P-ADP, while the methyl of the sulfonimide group has been speculated to occupy the ammonia binding site, based on early computerized mathematical analysis (14).

The binding of PPT or MetSox on GS has been further characterized by the following properties which underscore the mechanism of inhibition. (1) The binding of PPT is slow, 4 times slower than that of ATP (11). (2) The formation of the inactivation complex strengthens subunit–subunit inter-

[†] This work was supported by the National Institutes of Health (Grant GM-31299) and the Department of Energy (Grant DE-FC03-87ER60615).

* To whom correspondence should be addressed. Phone: (310) 825-3754. Fax: (310) 206-3914. E-mail: david@mbi.ucla.edu.

¹ Abbreviations: Glu~P, γ -glutamyl phosphate, also known as the intermediate of the biosynthetic reaction; Glu~P[ADP]-NH₃⁺, transition state in the biosynthetic reaction with ADP bound in the same active site; GS, glutamine synthetase; GS₁₂, fully adenylated glutamine synthetase; MetSox, L-methionine (S)-sulfoximine; MetSox~P, L-methionine (S)-sulfoximine phosphate; MetSox~P[ADP], L-methionine (S)-sulfoximine phosphate and ADP bound in the same active site; NCS, noncrystallographic symmetry; PPT, phosphinothricin; PPT~P, phosphinothricin phosphate.

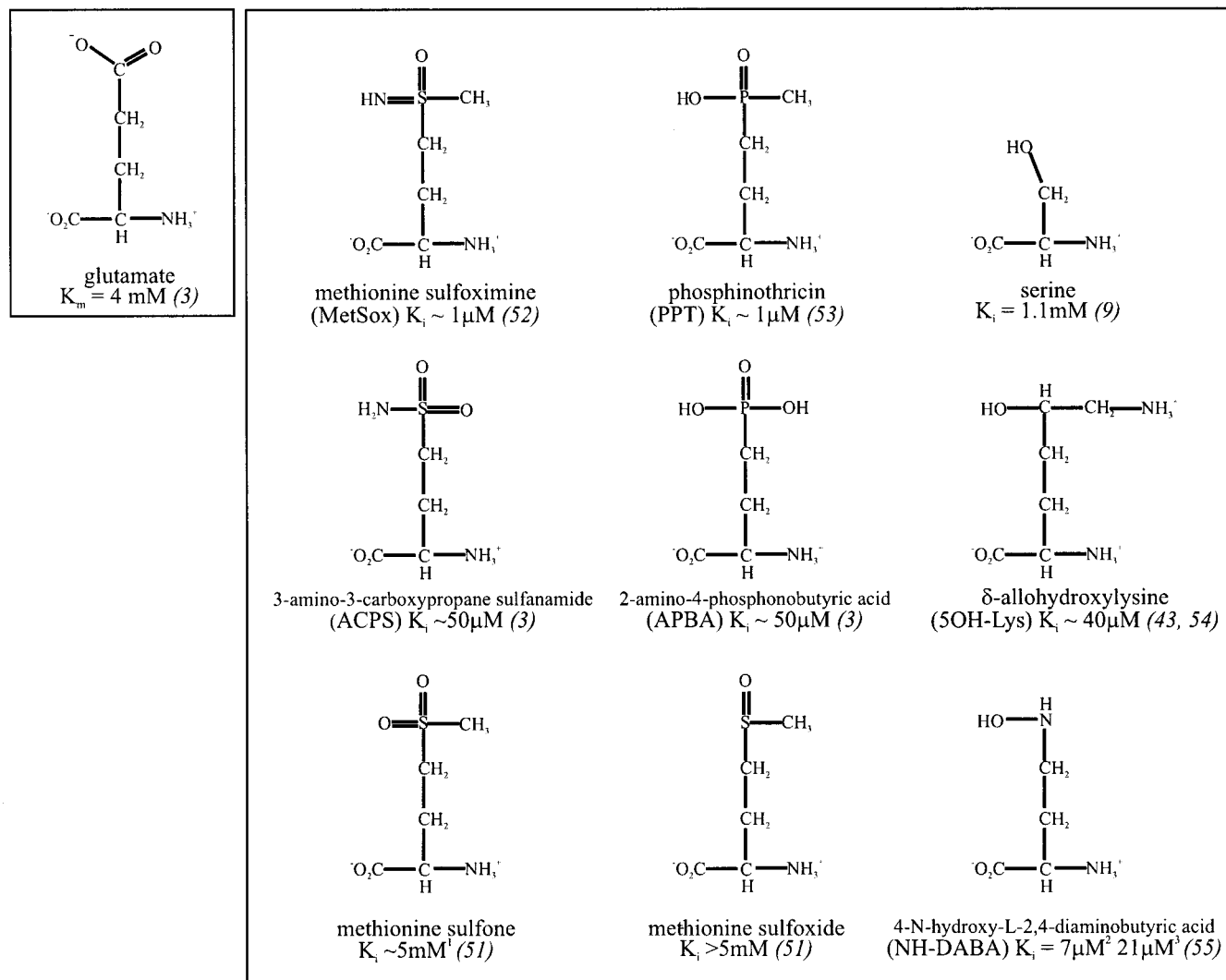


FIGURE 1: Glutamate analogues that inhibit GS. The compounds that are shown suggest that the presence of an H-bond donor at the ϵ -position is a characteristic of a good inhibitor for GS; MetSox, PPT, NH-DABA, 5OH-Lys, ACPS, and APBA are inhibitors of GS having dissociation constants in the low micromolar range. The X-ray crystallographic structures of PPT and MetSox bound in the active site of GS demonstrate that the H-bond donor at the ϵ -position on each inhibitor interacts with the Glu327 flap which sits at the glutamate entrance to the active site and closes the cavity. Binding of 5OH-Lys, of NH-DABA, of ACPS, and of APBA are predicted also to close the flap with their H-bond donor groups at the ϵ -position. Methionine sulfone and methionine sulfoxide display weaker binding for GS, having dissociation constants in the low millimolar range, perhaps reflecting the lack of a H-bond donor at the ϵ -position and thus an inability to interact with the flap. The binding of serine supports the hydrogen bond interaction between the inhibitor and the Glu327 flap; serine stabilizes the flap with its hydroxyl group as observed in the X-ray crystal structure of the GS-serine complex, whereas the electron density for the flap remains disordered in the GS-alanine complex (9). The difference in position between the hydroxyl group of serine (on the β -position) and the tighter binding inhibitors (on the δ -position) may explain the weaker dissociation constant for serine (9). ¹Estimated from the double-reciprocal plot in ref 51. ²Sheep brain GS. ³Soybean GS.

actions (18, 19), and tryptophan fluorescence is changed, as shown with MetSox (20). (3) The inactivation can be reversed by a variety of nondenaturing conditions, such as lowering the pH to 3.5–4.6 in 1 M KCl which protonates carboxylate groups or by brief heating which causes structural perturbations (21). The net result is the release of the metal ions, MetSox~P, and ADP. GS can be reactivated by returning the pH to 7 which results in the rebinding of these components to the enzyme and reflects a well-ordered mechanism of inactivation and subsequent reactivation (21).

EXPERIMENTAL PROCEDURES

Escherichia coli Strains and Culture Conditions. *S. typhimurium* GS was expressed in an *E. coli* recombinant system using glutamine auxotroph strain YMC21E of *E. coli* (Δ -

[glnA-glnG], glnE::TN5) (22, 23). This strain lacks adenylyltransferase activity and yields fully unadenylylated GS (24). All transformations were performed as described by Hanahan (25). Cultures were grown with the YMC21E strain in LB medium containing 50 $\mu\text{g}/\text{mL}$ ampicillin and 50 $\mu\text{g}/\text{mL}$ kanamycin, using a 150-L New Brunswick IF250 fermentor.

Purification of Recombinant S. typhimurium GS. Recombinant GS was purified by the procedure described by Woolfolk et al. (26) for *E. coli* GS isolation, omitting the following steps: heat treatment, acetone precipitation, and the second ammonium sulfate precipitation. An affigel-blue (Bio-Rad, 100–200 mesh) affinity column was used as the final purification step, as described by Janson et al. (27) for *S. typhimurium* GS isolation. This was followed by dialysis

Table 1: Summary of Diffraction Data and Atomic Refinement for Inhibited GS Molecules^a

	GS-ADP-Tl ^c	GS-ADP-PPT	GS-ADP
unit cell dimensions	231.1 Å × 132.8 Å × 196.8 Å, β = 102.4°	230.6 Å × 132.5 Å × 195.9 Å, β = 102.4°	230.6 Å × 132.5 Å × 195.9 Å, β = 102.4°
data			
resolution (Å)	2.67	2.89	2.49
no. of unique reflections (N)	130547	87421	196568
completeness (%)	82	70	98
<i>R</i> _{merge} ^b (%)	13	7.4	8.4
<i>R</i> _{iso} ^c (%)	15	20	N/A
<i>B</i> _{wilson}	44	53	46
no. of atoms in model			
protein (non-hydrogen)	43644	47280	43644
metal	48	24	24
water	840	1836	3504
refinement parameters			
resolution range (Å)	32–2.67	15–2.89	34.9–2.49
<i>R</i> -factor ^d (%)	23.3	24.8	24.3
<i>R</i> _{free} (%)	26.4	26.3	25.2
<i>B</i> _{ave}	46.3	49.0	52.2
deviation from ideality (rmsd)			
bonds (Å)	0.015	0.012	0.012
angles (deg)	2.22	1.9	1.91
dihedrals (deg)	25.4	24.9	25.0
impropers (deg)	1.87	1.82	2.03

^a The models were refined with strict 12-fold NCS constraints. Regions of the backbone with poor electron density correspond to highly flexible loops as discussed in the text and by Eisenberg et al. (43). ^b $R_{\text{merge}} = \sum(I - \langle I \rangle) / \sum I$, where I values are intensity measurements. ^c $R_{\text{iso}} = \sum_{hkl} (|F_{\text{derivative}} - F_{\text{native}}|) / \sum_{hkl} |F_{\text{native}}|$. ^d $R = 100(\sum |F_o - F_c|) / (\sum F_o)$, where F_o and F_c are the observed and calculated structure factors, respectively. ^e The thallium data set was taken in-house using an R-axis IV detector with a rotating anode generator, and compared to a similarly recorded native GS data set.

against 15 mM imidazole (pH 7) and 2.2 mM MnCl₂ until all the nucleotide from the elution buffer was removed as judged spectrophotometrically (28).

Crystal Soaking and Data Collection. GS crystals were grown by the hanging drop method of vapor diffusion and contained ADP (9). To prepare crystalline complexes, thallium acetate (1–5 mM) or D,L-phosphinothricin (100 mM) was dissolved in synthetic mother liquor and the solution slowly added to crystal-containing drops over a period of 5 min. Thallium–GS crystals when frozen for cryogenic data collection have essentially the same unit cell dimensions as the native form. X-ray data were recorded on an R-Axis IV detector with a rotating anode X-ray generator. The crystal-to-detector distance was set to 200 mm, and a helium box was used to reduce the level of air absorption. Exposure times were 30 min, and the oscillation angle was set to 1.1°. For the phosphinothricin soak, cryogenic data were collected at the X12C beamline at the National Synchrotron Light Source (Brookhaven National Laboratory, Upton, NY). Data were indexed and processed with the programs DENZO and SCALEPACK (29). Statistics for data collection are given in Table 1.

Fourier Difference Map Calculations. Twelve-fold NCS-averaged difference maps, using the Fourier coefficient relationship $|F_{o(\text{GS-inhibitor})} - |F_{o(\text{GS})}|$, were calculated using either the program XtalView (30) or the program suit RAVE (31). Phases from the refined structure of *S. typhimurium* GS at 2.5 Å were used in the calculation of the maps of the binary complexes. Atomic refinement was performed using the program XPLOR 3.843 (32), yielding the statistics listed in Table 1. The coordinates of the Tl⁺–GS model, the PPT–GS complex, and the 2.5 Å native structure have been deposited to the Protein Data Bank as entries 1F1H, 1FPY, and 1F52, respectively.

RESULTS

Two Main Tl⁺ Binding Sites per Active Site

To define the ammonium ion binding sites of GS more completely, X-ray data were collected from crystals of GS complexed with the ammonium analogue, thallos ion (33). Figure 2a shows the difference electron density map computed with coefficients $[|F_{o(\text{GS-Tl})} - |F_{o(\text{GS})}|]$ after 12-fold NCS averaging. Two density peaks are visible within each GS monomer. Panels b and c of Figure 2 show these peaks superimposed on a backbone chain representation of the dodecamer. The difference density peaks are situated in the bifunnel-like active sites. One of the peaks coincides with the ammonium substrate binding site as described by Liaw et al. (34). This peak is modeled as Tl473. The location of the other Tl⁺ ion peak, modeled as Tl474, coincides with the site of binding of the ammonium group of the substrate glutamate. Table 2 gives the separation of these cation binding sites. This second thallium peak was observed in weak density by Liaw et al. (34), with Asn264, Gly265, and Glu131 suggested as its ligands. The new map shows a strong peak at this same site and suggests that one water molecule also coordinates the ion, giving a total of four strong protein interactions with the thallium ion. Side-chain movements toward Tl474 are observed for Asn264 and Glu131. In addition, the side chain of Gln218 may also weakly coordinate the second thallium ion. All four of the residues that coordinate Tl474 are completely conserved in all known GS sequences.

Charge Asymmetry

A charge division within the bottom half of the bifunnel creates a positively charged pocket which stabilizes the substrate glutamate and a connecting negatively charged

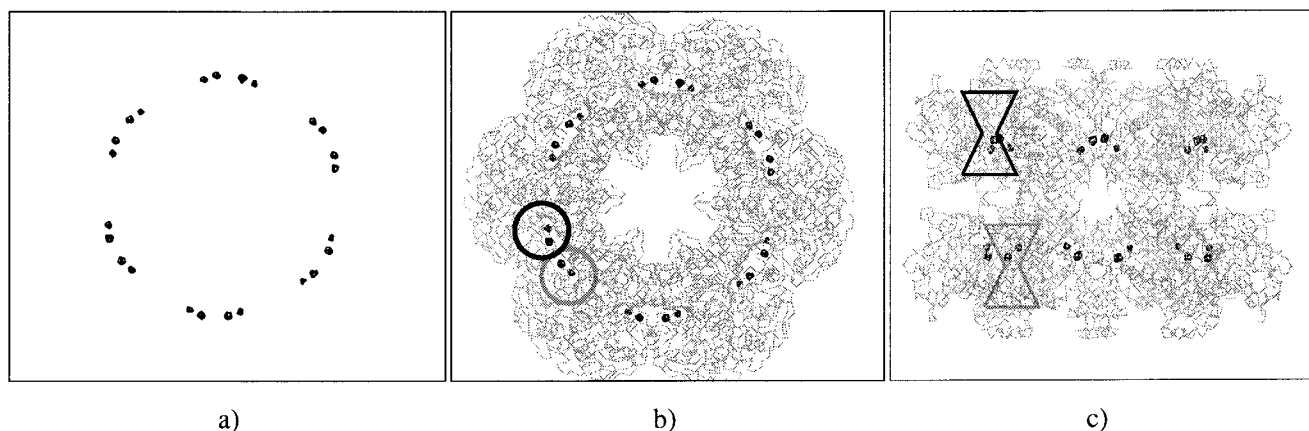


FIGURE 2: Thallium binding sites in each active site of GS. (a) Twenty-four electron density peaks are shown at a 14σ contour level in the GS–Tl⁺ dodecameric complex in the 12-fold NCS-averaged [$F_{o(GS-Tl)} - F_{o(GS)}$] Fourier difference map. $F_{o(GS-Tl)}$ is the observed structure factor from the GS–thallium ion binary complex data set, and $F_{o(GS)}$ is the observed structure factor from the native GS data set. One of the pair of closely spaced peaks is 39σ above the mean, and the other is 34σ above the mean. The peaks are the two highest in the averaged difference map, with the next highest peak 14σ above the mean. The higher of the two corresponds to the ammonium binding site where Tl473 binds, and the lower corresponds to a second ammonium ion binding site. (b and c) Top and side views, respectively, of the GS dodecamer are superimposed on the difference map, showing that the peaks lie in the active sites (or bifunnels) of GS. The black circle represents the mouth of a bifunnel on the upper hexameric ring and the gray circle that on the lower hexameric ring. The illustration was made using the program XtalView (30), and the peak heights were calculated with the program PEAKMAX (56).

Table 2: Metal–Metal and Metal–Ligand Separations in *S. typhimurium* GS

peak A	peak B	distance (Å) ^a	peak A	peak B	distance (Å) ^a
Mn470	Mn469	5.5	Asn264 (OD1)	Tl474	3.1
Mn470	Tl473	7.4	Gly265 (O)	Tl474	3.0
Mn470	Tl474	8.6	Glu131 (Oε1)	Tl474	3.6
Mn469	Tl473	3.8	Glu131 (Oε2)	Tl474	2.7
Mn469	Tl474	5.2	Gln218 (Oε1)	Tl474	4.2
Tl473	Tl474	5.6			

^a The error in atomic coordinates is ± 0.38 Å, as estimated by a Luzzati plot (50).

pocket that stabilizes ammonium (Figure 3). The ligands that form the negatively charged ammonium pocket include Glu212, Tyr179, Asp50', and Ser53', where the apostrophe means that the residue is on the adjacent subunit (34), and are confirmed by the map in Figure 4d. Another negatively charged pocket forms the binding site of Tl474 (Figure 4c); this site serves to bind the amino group of the substrate glutamate in the biosynthetic reaction. Both negatively charged pockets are situated on the same side of the bottom half of the bifunnel. The other side of the bottom half, which is positively charged, stabilizes the α - and γ -carboxylate groups of the substrate glutamate. This positively charged pocket is created by Arg331, Arg339, Arg344, Arg359, His269, and His270.

Phosphinothricin–GS Complex

Electron Density Map. Figure 4a shows the electron density of a 12-fold NCS-averaged GS–PPT difference electron density map, with a model of PPT built into it. The electron density of PPT was found to lie in the bifunnel, in the vicinity of the Tl⁺ ions, overlapping the glutamate binding site (9). Figure 4b shows the electron density of PPT in the bifunnel of GS, illustrating the effect of PPT binding on nearby residues. These affected residues have moved from their native positions, as shown by difference electron

density. The loop containing Glu327 (the Glu327 flap) is bound by the phosphinyl end of PPT, as is the side chain of Asn264. The Glu212 side chain shifts away from the polar site where Tl473 binds and is now rotated to the other side of the Mn469 ion. A pronounced shift turns the Tyr179 side chain away from the inside of the bifunnel. And the side chain of Asp50' appears to have moved away from the pocket as suggested by the difference density along the main chain. All residues displaying significant difference density are completely conserved in all known GS sequences. Residues Glu327, Glu212, Tyr179, and Asp50' but not Asn264 have been described to form the polar pocket which binds the ammonium substrate in the biosynthetic reaction (5).

Glu327 Flap and Orientation of the Phosphinyl Group in Phosphinothricin Binding. The orientation of the phosphinyl group can be inferred by the Glu327 flap stabilization. The Glu327 flap is defined as the loop segment consisting of residues 324–329 that guards the glutamate entrance into the bifunnel. The electron density for the Glu327 flap is not visible in the GS native structure or in the glutamate–GS complex (5). However, a strong density peak for the flap consistently appears when MetSox or PPT binds to GS. Because a major difference between glutamate and these inhibitors is their δ -groups, this suggests that there is interaction between the phosphinyl group of PPT with the Glu327 flap. For this reason, we oriented one phosphinyl oxygen (Oε2) of PPT toward the Glu327 flap, shown in Figure 5a. Using bond lengths for PPT obtained from the small molecule structure determination (35), we are able to estimate the distance between Oε2 and the carboxylate oxygen of Glu327 as 2.6 Å, the separation expected for a strong hydrogen bond. To form such a hydrogen bond, either Oε2 of PPT or the closer carboxylate oxygen of Glu327 must be protonated to provide a hydrogen bond donor. A protonated PPT is in agreement with the small molecule structure solutions of PPT, crystallized in an ethanol/water mixture (35) and in an aqueous solution with excess 20% hydrochloric acid (36).

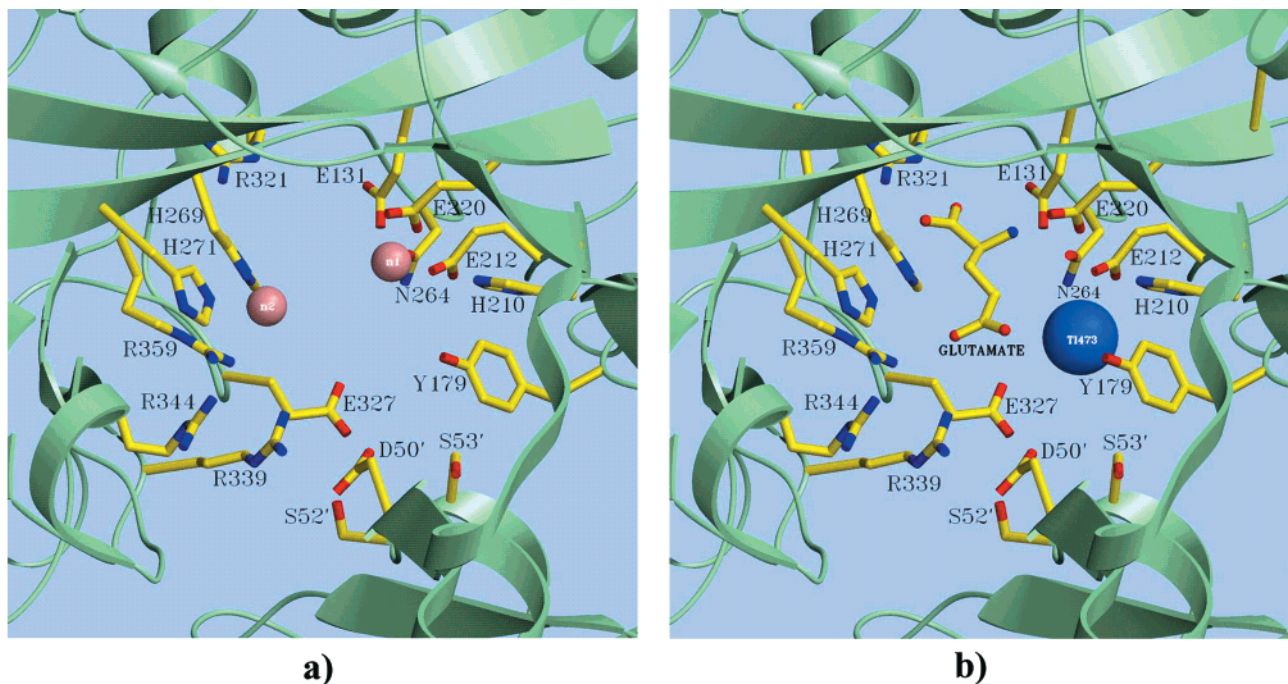


FIGURE 3: Charge asymmetry around the GS glutamate binding site. (a) The placement of all active site residues around the glutamate substrate binding site is shown from the native model, looking down the z -axis. The blue atoms represent nitrogens with hydrogens attached and the red atoms oxygens, and the green represents the secondary structures of the enzyme. Notice the charge separation, with positive charge on the left and negative on the right. (b) Two binding pockets are formed in the active site, one that binds the substrate glutamate (yellow) and one that binds T1473 (blue). The H-bond donor and acceptor groups on glutamate complement the charge asymmetry in the active site, as does the positive charge of T1473.

As illustrated in Figure 5a, the placement of the other phosphinyl oxygen (O ϵ 1) and the methyl group of PPT are restricted once O ϵ 2 has been oriented toward the Glu327 flap. The shift of Glu212 and Tyr179 away from the first ammonium binding site hints that the electronegative O ϵ 1 atom repels them. Furthermore, by orienting O ϵ 1 as shown and accepting the phosphinyl bond angles from the small molecule solution, we find the distance between Mn469 and O ϵ 1 to be 2.4 Å, affording significant electrostatic attraction. Alternatively, O ϵ 1 could be oriented toward the positively charged side of the bifunnel, where Arg339, Arg359, or His269 could act as a hydrogen bond donor to O ϵ 1. This would also make chemical sense, but perhaps weaker hydrogen bonding.

Flap Closure. Depicted in Figure 6, the Glu327 flap occludes the bottom entrance of the bifunnel, but only after PPT binds. The atomic displacement (B) factors in the native model for flap residues Gly325, Tyr326, and Glu327 are 100 Å², suggesting many conformations for the loop. Computational deletion of the Glu327 flap increases the total surface area of the enzyme by 300 Å², reflecting an increased opening of the active site cavity. In the PPT–GS complex, however, both PPT O ϵ 2 and Asn264 Nd1 stabilize Glu327 O ϵ 1 and O ϵ 2, respectively. The average B -factor for the Glu327 flap in the PPT–GS complex drops to 50 Å², with partial occupation of the active sites by the inhibitor. The stabilizing interactions of Glu327 with PPT are supported by further interactions along the bottom rim of the entrance site (Gly325 with Lys176, Tyr326 with Lys256 and Gly262), making the electron density for the entire loop visible. The entryway into the cavity is narrower and better complements the contour of the flap than in the native model. In short, PPT buries itself in the enzyme.

DISCUSSION

What Is the Similarity between PPT and MetSox Binding? Our model of PPT binding suggests the orientation of the sulfonamide group of MetSox on GS. Both PPT and MetSox binding stabilize the Glu327 flap and the Asn264 loop and in similar ways. Hence, we adjust the model of MetSox bound in the active site of GS from Liaw et al. (5) to parallel our model of PPT binding (Figure 5b). That is, the protonated N ϵ atom of MetSox hydrogen bonds with a carboxylate oxygen of Glu327. The carboxylate oxygen of Glu327 and the protonated N ϵ atom of MetSox are within hydrogen bonding distance. A distance of 2.6 Å was reported by Liaw et al. (5) as the closest distance between inhibitor density and the flap. This value is the same as the distance reported here between one of the carboxylate oxygens of Glu327 and O ϵ 2 of PPT. In addition, the δ -amino group of Asn264 hydrogen bonds with the other carboxylate oxygen of Glu327 (5). The rest of the sulfonamide group is modeled using the crystal structure of MetSox (37). The O ϵ –S–N ϵ angle of 120° places the O ϵ atom in proximity to the Mn469 ion, with the protonated N ϵ atom oriented directly toward Glu327. The methyl group faces away from the ammonium site. This fixes the O ϵ and methyl groups around the δ -atom of the inhibitors in similar orientations in both models. Notice that this adjustment does not necessarily orient N ϵ of the sulfonamide group away from the ATP binding site, because ATP extends toward this site from above.

What about Other Orientations of the Sulfonamide Group? Previously suggested orientations (5, 14) depicted in panels c and d of Figure 5 do not account for the Glu327 flap stabilization, nor do they complement the left to right charge division of the active site or the placement of the n1 metal ion. The early computer-assisted model in Gass et al. (14),

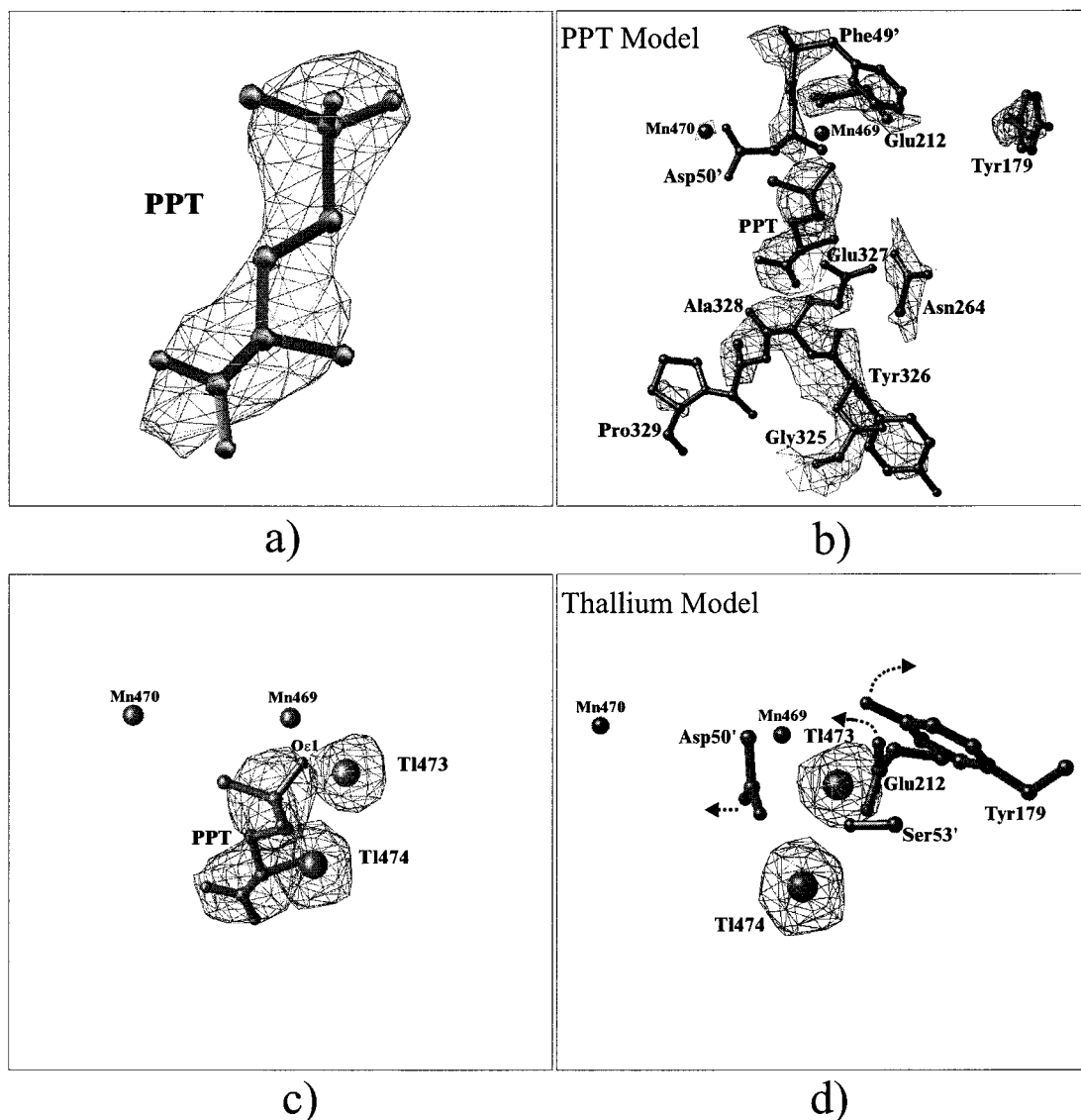


FIGURE 4: Phosphinothricin bound in an active site of GS. (a) The electron density of phosphinothricin (PPT) is shown as a 12-fold NCS-averaged $[F_{o(GS-PPT)} - F_{o(GS)}]$ Fourier difference map. $F_{o(GS-PPT)}$ is the observed structure factor amplitude from the GS-PPT binary complex crystal, and $F_{o(GS)}$ is the observed structure factor amplitude from the native GS crystal. The resolution of the map is 2.89 Å and is presented at a 10σ contour level. The highest peak of the entire map was found to lie in the top half of the density and the second highest peak in the lower half. The respective peak heights were 26σ and 18σ , with the next highest peak being 14σ above the mean. Superimposed in the density is a model of PPT. Model building of the main chain of PPT into the map was done by the phosphorus atom at the highest peak and the C α atom at the second highest peak. Notice the placement of atoms around the phosphorus atom. Because the three groups of atoms around the phosphorus are isoelectronic, the groups were placed by chemical reasoning (see the text). (b) The same map as in panel a, contoured at 6σ , shows the movements of active site ligands caused by the presence of PPT. The shapes of the densities make for easy identification of residues, although they are not apparent in this two-dimensional view. (c) With the same view of the active site as in panel b, the thallium complex map is shown, contoured at 14σ . For illustration, the model and electron density of PPT are superimposed on the thallium difference map. Notice that the amino group of PPT protrudes into the electron density of Tl474, a second ammonium binding site marked here by Tl $^+$. Notice also the proximity of the electron density of Tl473 to the δ -position of PPT. (d) The coordination of the Tl473 ion is shown in the same orientation as in panel b. The dotted arrows represent the direction of movement of the ligands which coordinate the polar pocket once PPT binds, as shown in panel b. The maps were made using the program XPLOR 3.843 (32), averaged with the program suit RAVE (31), and the peak heights were calculated with the program PEAKMAX (56).

on which both these orientations are based, described MetSox as a bifunctional reagent, apparently attaching to the enzyme at the sites for both glutamate and ammonia substrates. To arrive at this conclusion, Gass et al. (14) assumed features of substrate binding sites on GS. The most fundamental was that the location of the ATP binding site had to permit phosphorylation of the Ne group of MetSox from an adjacent site, the location of which relative to glutamate was deduced on the basis of binding studies of methyl-substituted, glutamate stereoisomers (38). The ammonia binding site was

placed with the help of another assumption: with the Ne group oriented toward this putative ATP binding site, the direction of the methyl group would then face toward the ammonia site, allowing for further speculation that the nature of the site had to be hydrophobic to accommodate the methyl group and shaping the idea that the methyl group acts as a substrate analogue for ammonia. MetSox binding would, therefore, mimic the tetrahedral geometry formed at the transition state, with the nucleophilic attack site occupied by the methyl of the sulfonamide group. With the attack site

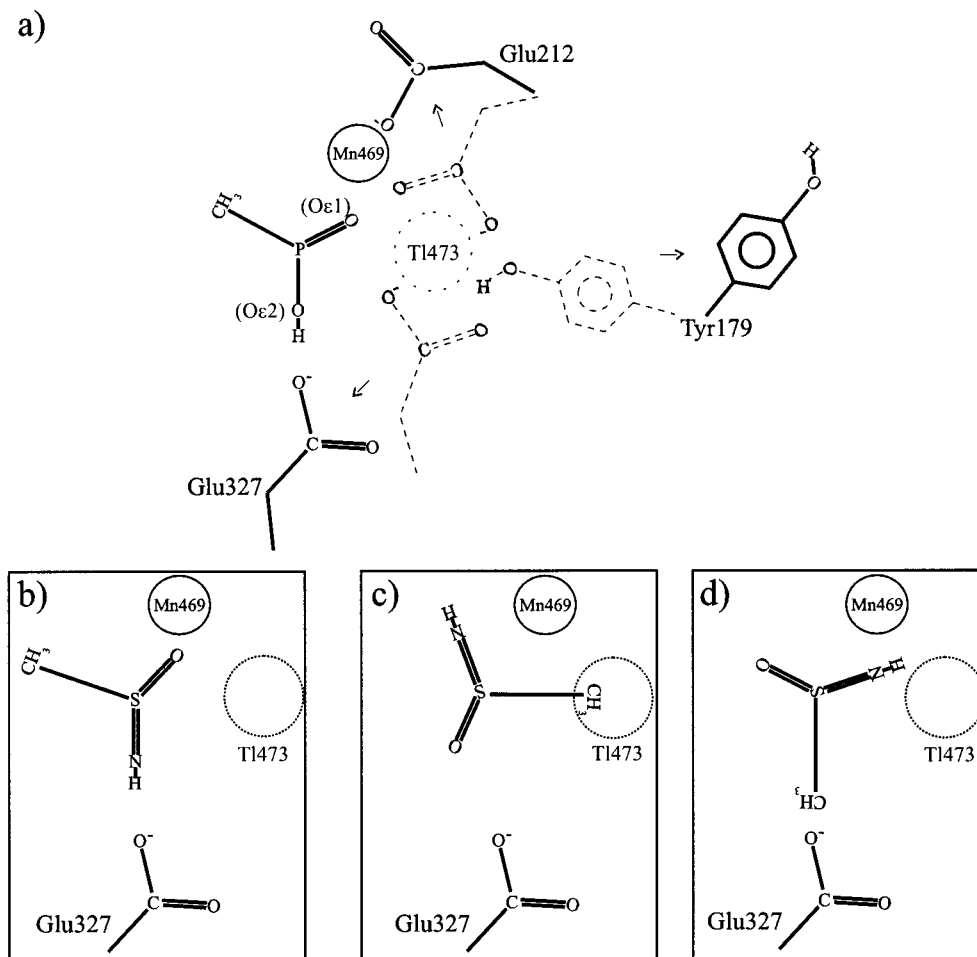


FIGURE 5: Proposed models for the orientation of the δ -groups of PPT and MetSox in the active site of GS. (a) The orientation of the phosphinyl group of PPT in the active site of GS is represented as a two-dimensional projection onto the page. To permit a hydrogen bond with Glu327, the O ϵ 2 phosphinyl oxygen is protonated and is oriented toward Glu327. The other phosphinyl oxygen (O ϵ 1) is oriented toward the ammonium pocket, marked by T1473, maximizing the interaction with Mn469. The distance between O ϵ 1 and the T1473 site is 1.5 Å which is less than the sum of the van der Waals radii of ammonium (~ 2 Å) and oxygen (~ 1.4 Å), reflecting the disruption of the pocket by PPT. The movements of the ligands which coordinate the pocket are shown by the directions of arrows. (b) The sulfonimide group of MetSox is remodeled from Liaw et al. (5) to parallel the orientation of the phosphinyl group of PPT in panel a. This orientation permits hydrogen bond interaction between the nitrogen of the sulfonimide group and the carboxylate side chain of Glu327, as well as electrostatic interaction between the oxygen atom of the sulfonimide group and Mn469. (c) The sulfonimide group is oriented with the methyl group protruding into the ammonium (T1473) pocket as described by Gass et al. (14). If the methyl group truly blocks the site of nucleophilic attack in the second step of glutamine biosynthesis by occupying this site, one would expect an apolar pocket at this site. However, the fact that T1473 can bind there demonstrates that the site is a negatively charged one, having several oxygens surrounding it. This implication has led us to believe that it is an ammonium ion rather than ammonia which binds to this site (34). (d) The sulfonimide group is oriented with the methyl group facing Glu327 as described by Liaw et al. (5). If the methyl group points toward Glu327, the distances between the γ -carboxylate group of Glu327 would be too far (~ 6 Å) for interaction, in general, with either N ϵ or O ϵ atom of the sulfonimide group which are the only possible atoms capable of interacting with Glu327. Furthermore, the atoms would be facing away from the flap which does not allow for H-bonding. In short, the protonated N ϵ atom is the only possibility for the sulfonimide group to act as an H-bond donor to Glu327. To do so, the N ϵ atom needs to face the flap as illustrated in panel b.

now known to be a negatively charged pocket having protein ligands placed tetrahedrally, an ammonium ion rather than ammonia is believed to be the substrate (34). And because the polar pocket stabilizing the ammonium binding site is destroyed when the inhibitor interacts with the Glu327 flap, the need for MetSox to mimic tetrahedral geometry at the transition state is unnecessary for explaining the strong inhibition.

How Is PPT~P Tightly Bound in the Active Site? The Glu327 flap appears to account for the tight binding of both PPT~P and MetSox~P to GS. Once phosphorylated, the inhibitors presumably retain essentially the same orientation in the active site as the nonphosphorylated models presented here. Additional support for this placement comes from EPR

studies which suggest that the O ϵ group of MetSox~P interacts with Mn469 (39). This is the same orientation as our model of MetSox. In particular, the N ϵ group is oriented toward the entrance of the glutamate binding site. Low-resolution X-ray crystallographic studies of MetSox~P indicated that the residues comprising the flap became visible (40). Because the N ϵ group of MetSox interacts with a closed flap and becomes phosphorylated, the phosphate could "lock" the flap closed by hydrogen bonding. By locking we mean that the inhibitor is hydrogen bonded to the Glu327 flap and possibly the Asp50' loop. Once phosphorylated, the protonated N ϵ atom of MetSox might donate its proton to Glu327, releasing itself of the net positive charge, but the now protonated Glu327 could still be held in position by the

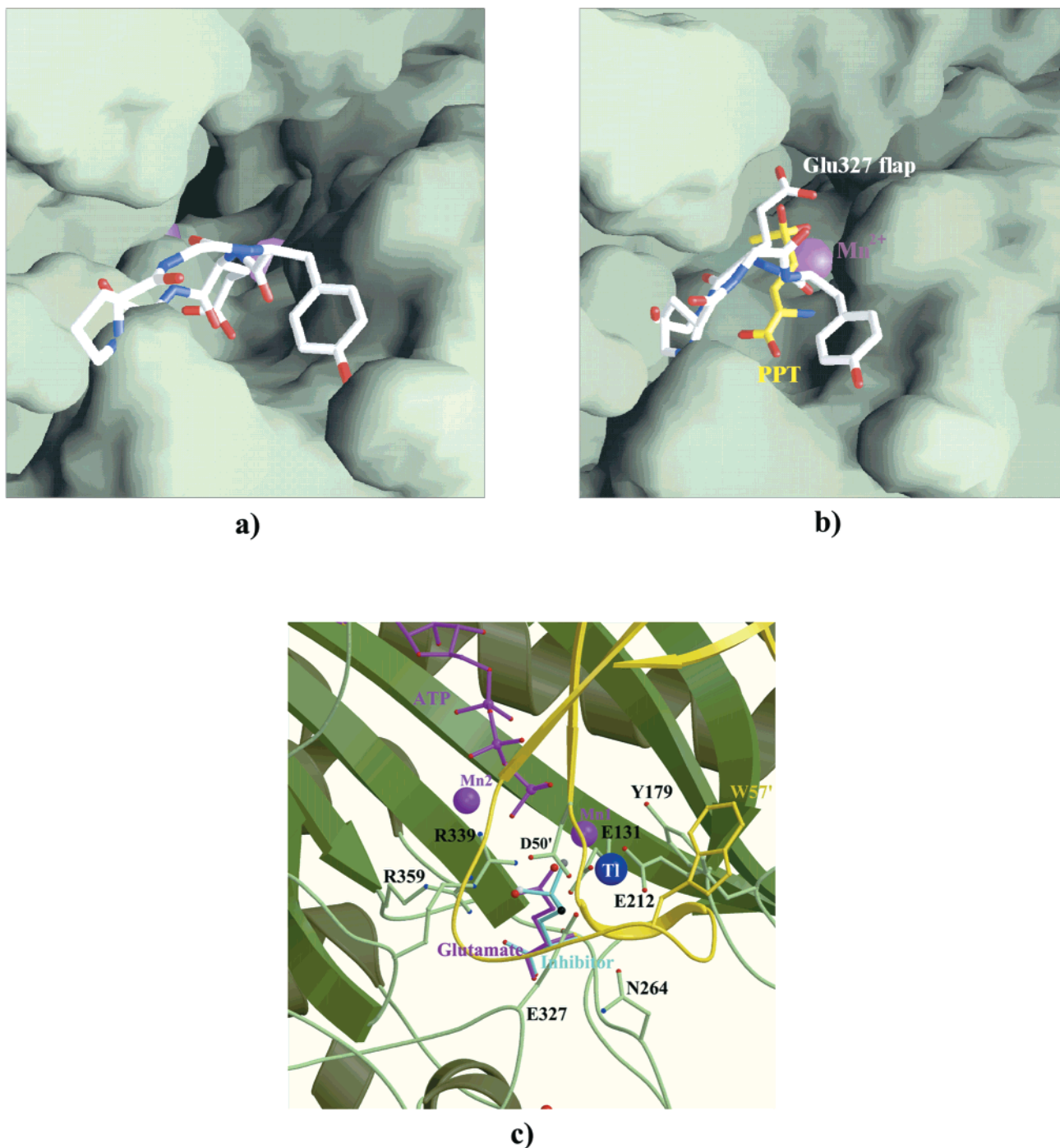


FIGURE 6: Open and closed models of the Glu327 flap and the GS active site. In panels a and b, the bottom entrance into the bifunnel is viewed, shown as a surface representation with the enzyme colored light green. The 6-fold axis of the enzyme is near vertical. The Glu327 flap is situated at the entrance and is shown as the white atomic model consisting of residues 325–328 of the enzyme. The catalytic manganese ions are represented by the violet spheres that are partially visible. The mechanism for the tight binding of PPT~P is illustrated by the comparison of the free enzyme (a) with the PPT–GS complex (b). In panel a, the Glu327 flap is seen to be down, allowing substrate entry into the active site (open). In panel b, PPT is shown trapped inside the cavity with Mn469 behind it (closed). If the flap were also a surface representation rather than an atomic model, the view into the cavity would now be seen to be completely blocked. Notice that the hydroxyl group at the ϵ -position of PPT faces Glu327 of the flap as if shutting the flap behind itself upon entry. By reference to the MetSox model described in the text, phosphorylation occurs on the oxygen of this hydroxyl group which creates an electrostatic attraction between the inhibitor and the carboxylate of Glu327 of the flap, thereby tightly binding PPT~P to GS. Notice also that the internal cavity seems to be less occluded than the native model. This reflects the movements of the loops which comprise the ammonium site ligands away from the ammonium binding site due to the proximity of PPT binding, that is, the disruption of the ammonium pocket. Panels a and b were made using the program GRASP (57). (c) The top view of the bifunnel is shown, with the 6-fold axis vertical as in Figure 2c. Because the bifunnels are formed between adjacent subunits within a ring of a hexamer, the green secondary structures are contributed by one subunit and the gold secondary structures are contributed by the adjacent subunit. To provide a clear view into the active site, the β -sheets on the gold subunit have been narrowed. The figure illustrates the binding of GS substrates and inhibitors, and suggests the movements of catalytic loops. Superimposed are models of the substrates ATP and glutamate (purple), the TI474 ion (dark blue), and a model of a generic tetrahedral inhibitor (light blue) which is used to closely represent PPT, MetSox, or APBA binding in the bifunnel. In the case of MetSox, the black ball at the ϵ -position is the protonated N ϵ atom, the white ball is a methyl group, and the gray ball is an oxygen atom. PPT differs from MetSox in that the black ball represents a hydroxyl group.

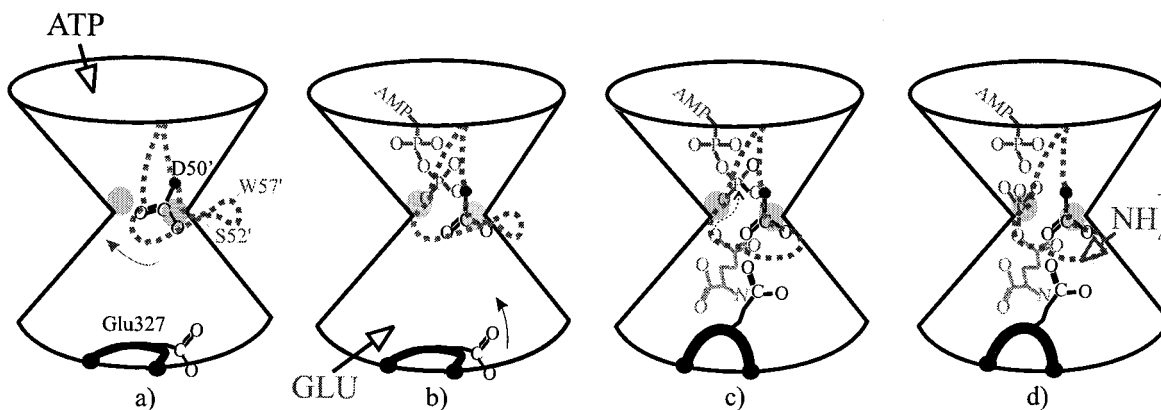


FIGURE 7: Mechanism of flap closure during glutamine synthesis. A cartoon of one active site of GS outlines our proposed mechanism for the first step in reaction 1. The gray circles at the neck of the bifunnel represent the metal ions; the dashed loop represents the Asp50 latch, and the black loop represents the Glu327 flap. The mechanism is described in the text.

phosphate group through hydrogen bond contacts, or by the electrostatic attraction between the electronegative Glu327 and the positive charge on the phosphorylated N ϵ atom. The biosynthetic reaction in the presence of MetSox or PPT comes to a dead end because the site for ammonia has been disrupted and nucleophilic attack on the δ -atom (the second step of reaction 1) can no longer occur.

What Prevents the Hydrolysis of the Enzyme-Bound Biosynthetic Intermediate? The closing of the Glu327 flap is the structural reason that the intermediate of reaction 1 remains stably bound to the enzyme. As the flap traps PPT and MetSox in the active site, the flap also shields the intermediate from aberrant hydrolysis. A possible mechanism for the closure of the Glu327 flap in reaction 1 can be seen in Figure 7. ATP enters from the top of the bifunnel, closing the Asp50' loop over the active site (a). Because Trp57' is located on this loop, the observed tryptophan fluorescence enhancement due to nucleotide binding (18, 20, 41) supports this conformational change in the Asp50' loop. This may position Ser52' to provide a hydrogen bond donor for the Glu327 flap. Glutamate now enters and binds above the Glu327 flap (still in the open position) and the Asn264 loop (b). The amino group of glutamate coordinates with the γ -carboxyl group of Asn264 (5). Both the γ -amino group of Asn264 and the hydroxyl group of Ser52' provide hydrogen bond donors for the γ -carboxylate of Glu327, thereby acting as "latches" for the flap. The flap completes the closure of the entry into the active site (c). The intermediate is formed and is shielded from solvent by the enzyme (42). In this process, Asp50' and Glu327 of the flap complete the upper polar pocket and increase the affinity for ammonium binding, allowing the second step of reaction 1 to proceed (d). In the absence of NH $_4^+$, this intermediate decomposes to ADP, free P $_i$, and glutamate (20), following opening of the flap over time. This model is supported by mutation of catalytic residues Asp50' and Glu327 which destabilize the formation of the intermediate and decrease the affinity for the NH $_4^+$ substrate (42). A cartoon of the mechanism in Eisenberg et al. (43) illustrates the complete reaction.

How Does PPT Binding Compare with That of Other Known GS Inhibitors? Figure 1 compares known inhibitors of GS to PPT and MetSox. Two in particular, ACPS and APBA, have been described as dead-end inhibitors of GS (3). The mechanism of inhibition of ACPS and APBA is

similar to that of MetSox and PPT in that they become phosphorylated by GS in the presence of ATP (3, 13). ACPS and APBA share two features with MetSox and PPT around the δ -position. Each has a group that can act as a hydrogen bond donor to the γ -carboxylate group of Glu327, and each has an electronegative atom to interact with Mn469. The structural similarity may be reflected in the similar K_i values (see Figure 1) for PPT and MetSox, in the low micromolar range, at least 2 orders of magnitude lower than the K_m for the substrate glutamate in *E. coli* GS. However, despite the resemblance among these inhibitors, a significant difference is that ACPS~P and APBA~P dissociate from GS in overnight dialysis at pH 7 (3, 13), whereas MetSox~P and PPT~P remain tightly bound. A possible explanation for this difference can be seen in Figure 6c. Notice that an oxygen atom on the δ -group of ACPS and APBA have replaced the methyl group in PPT and MetSox. This oxygen provides another site for phosphorylation. The oxygen (the white ball) overlaps with one of the two possible phosphorylation sites on the substrate glutamate (the red ball). Unlike the case of MetSox, where the methyl group occupies this space, phosphate transfer onto this oxygen of ACPS or APBA does not create electrostatic attraction to Glu327 of the flap. This difference in chemistry may cause the different rates of inactivation and dissociation of these inhibitors, because ACPS and APBA are not locked (11) in the active site by the flap.

How Common Are Catalytic Flaps and How Often Are They Associated with Tight Binding Ligands? A list of 12 enzymes containing catalytic flaps that close over their active sites can be found in Kempner (44). In common with the GS model presented here, the flaps have been described to trap ligands and limit active site exposure to solvent water. For example, the flaps in glutathione synthetase and in RuBisCo close over the active site to protect unstable intermediates formed during the course of their reactions (45, 46). Support for flap-closing mechanisms comes from tight ligand-protein complexes which mimic the intermediary states of catalysis. Another example is streptavidin which binds biotin tightly. A comparison of the crystal structures of streptavidin complexed to biotin and the apo structure revealed that a surface flap orders upon biotin binding, forming a hydrogen bond between biotin and the flap (47). In more recent examples, the structure of human hypoxanthine-guanine phosphoribosyltransferase is described as containing a catalytic loop that moves ~ 25 Å to cover the

active site upon binding a strong inhibitor (48). And, pepsin A (49) is described to have an essential H-bond between the inhibitor and the flap which aligns the substrate and facilitates the transition state.

In summary, the bottom half of the GS bifunnel is guarded by two main flexible loops, both destabilized in the holo form. Upon ATP and glutamate binding, the Asp50' latch cooperates with the Glu327 flap to close the active site, protecting the intermediate and completing the ammonium binding site. The PPT~P[ADP] complex whose structure is detailed here mimics the intermediate complex (Glu~P-[ADP]) of reaction 1.

ACKNOWLEDGMENT

We thank Dr. Thomas Sutherland for help in cell growth, Dr. Robert Sweet for help in data collection, Dr. Gaston M. U. Pfluegl for help in collecting the GS-ADP data set, and Dr. Ken Goodwill for discussion.

REFERENCES

- Krishnaswamy, P., Pamiljans, V., and Meister, A. (1962) *J. Biol. Chem.* 237, 2932-2940.
- Midelfort, C. F., and Rose, I. A. (1976) *J. Biol. Chem.* 251, 5881-5887.
- Meek, T. D., and Villafranca, J. J. (1980) *Biochemistry* 19, 5513-5519.
- Meister, A. (1980) in *Glutamine: Metabolism, Enzymology and Regulation of Glutamine Metabolism* (Palacios, R., and Mora, J., Eds.) pp 1-40, Academic Press, New York.
- Liaw, S. H., and Eisenberg, D. (1994) *Biochemistry* 33, 675-681.
- Bancroft, S., Rhee, S. G., Neumann, C., and Kustu, S. (1978) *J. Bacteriol.* 134, 1046-1055.
- Almassy, R. J., Janson, C. A., Hamlin, R., Xuong, N., and Eisenberg, D. (1986) *Nature* 323, 304-309.
- Yamashita, M., Almassy, R., Janson, C., Cascio, D., and Eisenberg, D. (1989) *J. Biol. Chem.* 264, 17681-17690.
- Liaw, S. H., Pan, C., and Eisenberg, D. (1993) *Proc. Natl. Acad. Sci. U.S.A.* 90, 4996-5000.
- Valentine, R. C., Shapiro, B. M., and Stadtman, E. R. (1968) *Biochemistry* 7, 2143-2152.
- Abell, L. M., and Villafranca, J. J. (1991) *Biochemistry* 30, 6135-6141.
- Colanduoni, J. A., and Villafranca, J. J. (1986) *Bioorg. Chem.* 14, 163-169.
- Logusch, E. W., Walker, D. M., McDonald, J. F., and Franz, J. E. (1989) *Biochemistry* 28, 3043-3051.
- Gass, J., and Meister, A. (1970) *Biochemistry* 9, 1380-1390.
- Weisbrod, R. E., and Meister, A. (1973) *J. Biol. Chem.* 248, 3997-4002.
- Shrake, A., Whitley, E., and Ginsburg, A. (1980) *J. Biol. Chem.* 255, 581-589.
- Shrake, A., and Ginsburg, A. (1982) *J. Biol. Chem.* 257, 8238-8241.
- Maurizi, M. R., and Ginsburg, A. (1982) *J. Biol. Chem.* 257, 7246-7251.
- Haschemeyer, R., Wall, J., Hainfield, J., and Maurizi, M. (1982) *J. Biol. Chem.* 257, 7252-7253.
- Timmons, R., Rhee, S., Luteran, D., and Chock, P. (1974) *Biochemistry* 13, 4479-4485.
- Maurizi, M. R., and Ginsburg, A. (1982) *J. Biol. Chem.* 257, 4271-4278.
- Chen, Y., Backman, K., and Magasanik, B. (1982) *J. Bacteriol.* 250, 214-220.
- Bowie, J., and Eisenberg, D. (1989) unpublished results.
- Ginsburg, A. (1972) *Adv. Protein Chem.* 26, 1-79.
- Hanahan, D. (1983) *J. Mol. Biol.* 166, 557-580.
- Woolfolk, C. A., Shapiro, B., and Stadtman, E. R. (1966) *Arch. Biochem. Biophys.* 116, 177-192.
- Janson, C. A., Almassy, R. J., Westbrook, E. M., and Eisenberg, D. (1984) *Arch. Biochem. Biophys.* 228, 512-518.
- Ginsburg, A., Yeh, J., Hennig, S., and Denton, M. (1970) *Biochemistry* 9, 633-649.
- Otwinowski, Z., and Minor, W. (1996) *Methods Enzymol.* 276, 307-326.
- McCree, D., Shah, A., Israel, M., and Pique, M. (1995) *XtalView*, version 3.0, The Computational Center for Macromolecular Structures at San Diego Supercomputer Center, La Jolla, CA.
- Kleywegt, G. J., and Jones, T. A. (1999) *Acta Crystallogr. D55*, 941-944.
- Brunger, A. (1992) *XPLOR Manual*, version 3.843, Department of Molecular Biophysics and Biochemistry, Yale University, New Haven, CT.
- Stroud, R. M., Kay, L. M., and Dickerson, R. E. (1974) *J. Mol. Biol.* 83, 185-208.
- Liaw, S. H., Kuo, I., and Eisenberg, D. (1995) *Protein Sci.* 4, 2358-2365.
- Paulus, E., and Grabley, S. (1982) *Z. Kristallogr.* 160, 63.
- Sawka-Dobrowolska, W. (1988) *Acta Crystallogr. C44*, 2193-2195.
- Chevrier, B., Moras, D., Jeannoda, V., Creppy, E., and Dirheimer, G. (1986) *Acta Crystallogr. C42*, 1632.
- Kagan, H., and Meister, A. (1966) *Biochemistry* 5, 2423-2432.
- Eads, C., LoBrutto, R., Kumar, A., and Villafranca, J. J. (1988) *Biochemistry* 27, 165-170.
- Jun, G. (1993) Ph.D. Thesis, Figure 3.3a, University of California, Los Angeles, CA.
- Atkins, W. M., Stayton, P. S., and Villafranca, J. J. (1991) *Biochemistry* 30, 3406-3416.
- Alibhai, M., and Villafranca, J. (1994) *Biochemistry* 33, 682-686.
- Eisenberg, D., Gill, H. S., Pfluegl, G. M. U., and Rotstein, S. H. (2000) *Biochim. Biophys. Acta* 1477, 122-145.
- Kempner, E. S. (1993) Minireview. *FEBS Lett.* 326, 4-10.
- Tanaka, T., Kato, H., Nishioka, T., and Oda, J. (1992) *Biochemistry* 31, 2259-2265.
- Schreuder, H. A., Knight, S., Curmi, P. M., Andersson, I., Cascio, D., Branden, C. I., and Eisenberg, D. (1993) *Proc. Natl. Acad. Sci. U.S.A.* 90, 9968-9972.
- Weber, P. C., Ohlendorf, D. H., Wendoloski, J. J., and Salemme, F. R. (1989) *Science* 243, 85-88.
- Shi, W., Li, C. M., Tyler, P. C., Furneaux, R. H., Grubmeyer, C., Schramm, V. L., and Almo, S. C. (1999) *Nat. Struct. Biol.* 6, 588-593.
- Okoniewska, M., Tanaka, T., and Yada, R. Y. (1999) *Protein Eng.* 12, 55-61.
- Luzzati, V. (1952) *Acta Crystallogr.* 5, 802-810.
- Ronzio, R., Rowe, W., and Meister, A. (1969) *Biochemistry* 8, 1066-1075.
- Logusch, E. W., Walker, D. M., McDonald, J. F., Franz, J. E., Villafranca, J. J., DiIanni, C. L., Colanduoni, J. A., Li, B., and Schineller, J. B. (1990) *Biochemistry* 29, 366-372.
- Walker, D. M., McDonald, J. F., and Logusch, E. W. (1987) *J. Chem. Soc., Chem. Commun.*, 1710-1711.
- Rabinovitz, M., Olson, M., and Greenberg, D. (1957) *Cancer Res.* 17, 885-889.
- Fushiya, S., Maeda, K., Funayama, T., and Nozoe, S. (1988) *J. Med. Chem.* 31, 480-483.
- Collaborative Computing Project, Number 4 (1994) *Acta Crystallogr. D50*, 760-763.
- Nicholls, A., Sharp, K. A., and Honig, B. (1991) *Proteins* 11, 281-296.

BI002438H